Published in final edited form as:
Mol Cell. 2013 May 9; 50(3): 437–443. doi:10.1016/j.molcel.2013.03.017.

Evidence that ribonucleotides are signals for mismatch repair of leading strand replication errors

Scott A. Lujan, **Jessica S. Williams**, **Anders R. Clausen**, **Alan B. Clark**, and **Thomas A. Kunkel***
Laboratory of Molecular Genetics and Laboratory of Structural Biology National Institute of Environmental Health Sciences, NIH, DHHS, Research Triangle Park, NC 27709, U. S. A.

Abstract

To maintain genome stability, mismatch repair of nuclear DNA replication errors must be directed to the nascent strand, likely by DNA ends and PCNA. Here we show that the efficiency of mismatch repair in *Saccharomyces cerevisiae* is reduced by inactivating RNase H2, which nicks DNA containing ribonucleotides incorporated during replication. In strains encoding mutator polymerases, this reduction is preferential for repair of mismatches made by leading strand DNA polymerase ε as compared to lagging strand DNA polymerase δ. The results suggest that RNase H2-dependent processing of ribonucleotides transiently present in DNA after replication may direct mismatch repair to the continuously replicated nascent leading strand.

INTRODUCTION

Mismatch repair (MMR) corrects DNA replication errors in the newly synthesized strand (Iyer et al., 2006; Kunkel and Erie, 2005). In order to enhance genome stability, MMR must be targeted to the nascent strand by one or more strand-discrimination signals. In *E. coli* and closely related bacteria, the nascent strand is marked for repair when, immediately after replication, MutH endonuclease nicks the DNA backbone at transiently under-methylated adenines in GATC sequences (Iyer et al., 2006). Moreover, a nick in DNA can signal for strand-specific eukaryotic MMR *in vitro* (Holmes et al., 1990; Thomas et al., 1991). However, the identity of the DNA ends used for strand discrimination during nuclear DNA replication *in vivo* is uncertain. Discontinuous lagging strand synthesis of Okazaki fragments (about 200 base pairs long in eukaryotes) produces transient 5′-DNA ends (Burgers, 2009), which have been implicated in discrimination for lagging strand replication errors (Nick McElhinny et al., 2010a; Pavlov et al., 2003). In contrast, the leading strand is likely to be replicated in a more continuous manner (Burgers, 2009). This raises the issue of the identity of the eukaryotic strand discrimination signal for MMR of leading strand replication errors.

We have suggested that ribonucleotides incorporated by DNA polymerases during replication might mark nascent strands for MMR (Nick McElhinny et al., 2010c). This hypothesis was based on several observations. *S. cerevisiae* replicases DNA polymerases α, δ and ε, (Pols α, δ and ε) frequently incorporate ribonucleotides into DNA *in vitro* (Nick McElhinny et al., 2010c). Pol ε incorporates ribonucleotides during replication *in vivo* (Nick

*Correspondence: kunkel@niehs.nih.gov.

McElhinny et al., 2010b), and does so preferentially into the nascent leading strand (Lujan et al., 2012). Most ribonucleotides incorporated during DNA replication are present only transiently, being efficiently repaired by Ribonucleotide Excision Repair (RER). RER is initiated when RNase H2 nicks the DNA backbone at ribonucleotides (Eder and Walder, 1991; Eder et al., 1993; Nick McElhinny et al., 2010b; Rydberg and Game, 2002; Sparks et al., 2012). Here we test whether this RNase H2-dependent processing of ribonucleotides provides a strand discrimination signal for MMR of leading strand replication errors.

RESULTS

The pol ε mutator incorporates ribonucleotides during leading strand synthesis

The *POL2* gene encodes Pol ε, which participates in leading strand replication (Pursell et al., 2007). We began by quantifying the density of ribonucleotides in the nascent leading strand *in vivo* in strains encoding a *pol2-M644G* variant. Compared to wild type Pol ε, M644G Pol ε incorporates 16-fold more ribonucleotides into DNA during synthesis *in vitro* (Figure 1A, data combined from (Nick McElhinny et al., 2010b; Williams et al., 2012)). Increased ribonucleotide incorporation also occurs *in vivo*, where these ribonucleotides can be detected as alkali-sensitive sites in the genomic DNA of strains that are defective in RER (Nick McElhinny et al., 2010b) due to deletion of the *RNH201* gene encoding the catalytic subunit of RNase H2. Consistent with Pol ε's role as a primarily leading strand replicase, strand-specific probing of DNA fragments generated by alkaline hydrolysis (Figure 1B and also see (Miyabe et al., 2011) for results in *S. pombe*) demonstrates that ribonucleotides are preferentially incorporated into the nascent leading strand (Figures 1C–D, and (Lujan et al., 2012)). Quantification of the DNA fragments (Figure S1) indicates that one ribonucleotide is introduced per about 950 base pairs (average of four independent experiments).

MMR efficiency is reduced in pol ε mutator strains lacking RNase H2

Pol ε M644G is less accurate than wild type Pol ε during DNA synthesis *in vitro*, and *pol2-M644G* strains are leading strand-specific mutators for single base substitutions and insertions/deletions (indels) (Lujan et al., 2012; Pursell et al., 2007). To determine if loss of RER reduces the efficiency of MMR of leading strand replication errors, we determined mutation rates for resistance to 5-fluoroorotic acid (5-FOA; toxic to *URA3* strains) in *pol2-M644G* strains harboring the *URA3* mutational reporter gene in each of two orientations (designated OR1 and OR2). We then determined *URA3* reporter gene sequences from independent 5-FOA resistant clones (Table 1) and used the data to calculate specific rates for single base transitions and indels, the two types of mutations that are most characteristic of an MMR defect (Lujan et al., 2012; Nick McElhinny et al., 2008; Nick McElhinny et al., 2010a). Defining this signature for loss of MMR is critical, because loss of RNase H2 elevates rates for another type of mutation, 2–5 base pair deletions (Nick McElhinny et al., 2010b), which occur via nicking by Topoisomerase 1 (Top1) after replication (Kim et al., 2011) and are not subject to mismatch repair (Clark et al., 2011). We compared transition and indel rates for *pol2-M644G msh6*Δ strains lacking MutSα (Msh2-Msh6)-dependent MMR (Figure 2A, upper panel) to rates for isogenic *pol2-M644G MSH6* MMR-proficient strains (Figure 2A, middle panel). The ratio of these rates provides MMR correction factors (Figure 2A, lower panel). We asked if the correction factors for these leading strand replication errors decreased in RER-deficient (*rnh201*Δ) strains, as predicted by the hypothesis that RER-dependent processing may provide a strand discrimination signal for MMR.

In the absence of RNase H2, correction factors in OR1 strains were reduced by 8.2-fold and 5.0-fold for transitions and indels respectively (Figure 2A, values below lower panel). To determine if this reduction was reproducible, an independent set of measurements (Table 1)

was made in *pol2-M644G* strains in which the location of *URA3* was preserved (adjacent to replication origin *ARS306*) but the *URA3* gene orientation was reversed (OR2). In these strains, Pol ε M644G replicates the complementary strand, providing completely different sequence contexts for incorporating ribonucleotides and for generating and repairing mismatches. Correction factors for transitions and indels in these strains were again reduced in the absence of RNase H2, this time by 2.5-fold and 25-fold, respectively (Figure 2A). These reductions are statistically significant ($p < 0.05$).

Similar reductions in MMR correction were observed when the experiments were repeated with *msh3*Δ *msh6*Δ strains that lack both MutSα-dependent and MutSβ (Msh2-Msh3)-dependent MMR. This included comparing *msh3*Δ *msh6*Δ strains to *msh3*Δ strains (Table S1 and Figure 2A bottom, with one exception for indels in OR1, where the p values was 0.43), as well as comparing *msh3*Δ *msh6*Δ strains to MMR-proficient strains (Table S2, upper panel). Because rates in *msh2*Δ strains are similar to rates in *msh3*Δ *msh6*Δ strains, similar reductions in MMR efficiency were observed using rates from *msh2*Δ strains (Table S2, lower panel) that also lack MutSα-dependent and MutSβ-dependent MMR.

MMR efficiency is not reduced in Pol δ mutator strains lacking RNase H2

Genetic evidence in *S. cerevisiae* (Nick McElhinny et al., 2010a; Pavlov et al., 2002) led us to previously suggest that the 5′-DNA ends of Okazaki fragments, perhaps in conjunction with PCNA, may be used as signals for strand discrimination during MMR. These 5′ ends are transiently present about every 200 base pairs ((Burgers, 2009; Smith and Whitehouse, 2012) and references therein). This density is about 5 to 10 -fold higher than for ribonucleotides in the nascent leading strand in the *pol2-M644G rnh201*Δ strains (Figures 1A and 1D). This led us to hypothesize that loss of RNase H2-dependent processing of ribonucleotides will have a lesser role in strand discrimination during lagging strand replication. To test this, we used the L612M mutator variant of Pol δ. Pol δ L612M is a mutator polymerase (Nick McElhinny et al., 2007) with a base substitution and indel error signature characteristic of lagging strand replication (Nick McElhinny et al., 2008). We now report that Pol δ L612M also incorporates 10-fold more ribonucleotides into DNA during synthesis *in vitro* than does wild type Pol δ (Figure 1A), and that this property is manifested *in vivo* as an increased number of strand-specific alkali-sensitive sites in DNA isolated from *pol3-L612M rnh201*Δ strains (Figures 1B–C). However in this case, the ribonucleotides are preferentially observed in the nascent lagging strand (Figures 1C–D,). This supports the interpretation, based earlier on mutational signatures (Larrea et al., 2010; Nick McElhinny et al., 2008), that Pol δ is primarily a lagging strand replicase. The density of alkali-sensitive sites in the *pol3-L612M rnh201*Δ strain (Figure S1) further indicates that one ribonucleotide is present per about 3400 base pairs. At this density, incisions by RNase H2 are expected to have little effect on the total number of transient DNA ends in the nascent strand compared to those already resulting from Okazaki fragment synthesis. Consistent with this, mutational analyses with *pol3-L612M* strains (Table S3), analogous to those described above for *pol2-M644G* strains, indicated that loss of RNase H2 did not *decrease* the efficiency of MutSα-dependent MMR of transition and indel mismatches generated by L612M Pol δ (Figure 2B). Instead, there are small *increases* in MMR efficiency in the *pol3-L612M rnh201*Δ strains. These increases are statistically significant in one *URA3* orientation (OR2, $p \leq 0.021$), but not in the other (OR1, $p > 0.23$).

Indel MMR efficiency is reduced in RNase H2-defective strains with wild type replicases

Does RNase H2 status affect MMR efficiency in strains with wild type Pols δ and ε? To test this, we examined the number of alkali-sensitive sites in DNA isolated from *rnh201*Δ strains encoding wild type polymerases. The results (Figures 1C–D) suggest that one ribonucleotide is present in the nascent leading strand per about 6500 deoxyribonucleotides. When

mutational analyses similar to those described above were performed in strains encoding wild type polymerases (Table S4), the results showed that loss of RNase H2 decreased the efficiency of MutSα-dependent MMR of indel mismatches (Figure 2C) by 4.1-fold in OR1 strain ($p \leq 0.001$) and by 2-fold in OR2 strains ($p = 0.069$), with no significant effect on MMR of transitions. The decrease in MMR efficiency for indels but not transitions is consistent with many studies showing that indels are more sensitive biomarkers for a eukaryotic MMR deficiency than are transitions. This applies to our own studies in yeast strains with wild type replicases, where the majority of uncorrected replication errors are single base deletions in mononucleotide runs (7) that are corrected at least 10 times more efficiently than transitions.

MMR efficiency is largely unaffected in a strain containing fewer ribonucleotides in DNA

The hypothesis that ribonucleotides direct MMR to the nascent leading strand predicts that reducing the number of ribonucleotides incorporated into DNA will reduce the effect of deleting *RNH201* on MMR efficiency. To test this prediction, we measured spontaneous mutation rates and mutational specificity in *pol2-M644L* strains that contain fewer genomic ribonucleotides than *POL2* and *pol2-M644G* strains (Nick McElhinny et al., 2010b). The mutation data (Table S7) were then used to calculate the difference in single-base indel rate in *rnh201*Δ versus *RNH201* strains. This difference in the *pol2-M644L* strain is a negligible 1.1-fold (Figure 2D, blue bar on left, and Table S7), indicating that RNase H2 status is irrelevant in the *pol2-M644L* strain, which exhibits diminished genomic ribonucleotide incorporation. This 1.1-fold difference is significantly lower than the 3.2-fold difference in the *POL2* strain (red bar; $p = 0.019$). An even greater difference (10-fold; green bar) is observed in the *pol2-M644G* strain, which contains the greatest number of ribonucleotides in the genome. Importantly, *RNH201* deletion has no significant effect on single-base indel rates in MMR-deficient strains in the *pol2-M644G* background (Figure 2A and Table S1). Assuming this is also true in the *POL2* and *pol2-M644L* strains, the results for single-base indels in Figure 2D strongly support the hypothesis that ribonucleotides in the nascent leading strand are important for repairing replication errors in that strand. Serving as a positive control in these experiments are results for 2–5 base pair deletions from direct repeats in the same three strains. The effect of *RNH201* deletion on the rate of these events, which are due to topoisomerase 1-dependent cleavage of unrepaired ribonucleotides incorporated into DNA (Kim et al., 2011), is highest in the *pol2-M644G rnh201*Δ strain, intermediate in the *POL2 rnh201*Δ strain, and lowest in the *pol2-M644L rnh201*Δ strain (Figure 2D, right). The latter result confirms recent observations (Cho et al.).

DISCUSSION

The results in the M644G Pol ε background (Figure 2A), and to a lesser extent in the wild type (Figure 2C) and M644L Pol ε backgrounds (Figure 2D), are consistent with the idea that RNase H2-dependent processing of ribonucleotides incorporated by Pol ε may direct MMR to correct mismatches made during continuous leading strand replication. Thus RNase H2 action on ribonucleotides transiently present in the nascent leading strand may generate strand discrimination signals in a manner akin to transiently under-methylated adenines in GATC sequences and MutH endonuclease in *E. coli*. A simple explanation is that RNase H2 nicks the DNA backbone at positions of newly incorporated ribonucleotides, allowing these nicks to serve as strand discrimination signals, and possibly as entry points for removing mismatches.

Removal could occur by excising the nascent strand containing the mismatch, e.g., by exonuclease 1, or removal could occur by DNA synthesis to displace the nascent strand containing the mismatch followed by cleavage of the 5′-DNA flap (Kadyrov et al., 2009). In fact, the latter mechanism operates during ribonucleotide excision repair (Sparks et al.,

2012). An additional attractive feature of the RNase H2-dependent signaling model is that the non-catalytic B subunit of RNase H2 contains a PCNA binding motif (Chon et al., 2009). PCNA directs RNase H2 to replication foci and imposes strand specificity on its function (Bubeck et al., 2011). PCNA is required for RER (Sparks et al., 2012), and it also required for early steps in MMR (Umar et al., 1996), where it has been implicated in signaling for strand discrimination (see (Pluciennik et al., 2010) and references therein) Thus, in addition to initiating RER, RNase H2 may deliver PCNA in an orientation-dependent manner to the nascent leading strand after replication in order to participate in signaling for MMR.

Our estimates of the density of ribonucleotides in the leading strand template are based on probing the *URA3* locus, which is only a tiny fraction of the yeast genome (Figure 1B). Because ribonucleotide incorporation by Pol ε varies considerably with sequence context and ribonucleotide identity (Nick McElhinny et al., 2010b), ribonucleotide density *in vivo* could differ elsewhere in the genome. Nonetheless, in the *URA3* reporter gene adjacent to *ARS306*, ribonucleotide density is sufficient to introduce nicks at intervals consistent with excision between the signal and the mismatch, which can cover a distance of 1,000 base pairs (Fang and Modrich, 1993). Moreover, a nick introduced by RNase H2 need not necessarily be the starting point for excision *per se*, but could rather be the signal needed for directing the endonuclease activity of the hPms2/yPms1 subunit of MutLα to introduce nicks that can be used for excision (Kadyrov et al., 2006; Kadyrov et al., 2007).

It is also important to note that mutation rates for transitions and indels in the *pol2-M644G* background are much higher when MMR is completely inactivated, as in *msh3*Δ *msh6*Δ strains (Table S2, upper panel) and *msh2*Δ strains (Table S2, lower panel), than are rates in *rnh201*Δ strains lacking RNase H2 (Table 1). Thus, while nicking by RNase H2 may contribute to signaling for MMR of leading strand errors, one or more other signals are likely to exist. Given the importance of MMR to genome stability, redundant signals are to be expected. Candidate signals include the 3′-DNA ends used for chain elongation and/or PCNA (e.g., (Hombauer et al., 2011; Kleczkowska et al., 2001; Kunkel and Erie, 2005; Modrich and Lahue, 1996; Pavlov et al., 2003; Pluciennik et al., 2010; Tran et al., 1999; Umar et al., 1996)).

Sequence alignments (Figure 3) show that the amino acid in yeast Pol δ that was changed in this study, Leu612, is invariant among all Pols δ. When changed to methionine, L612M Pol δ becomes promiscuous for ribonucleotide incorporation (Figure 1). Thus, this lagging strand replicase conserves a leucine that helps to prevent ribonucleotide incorporation. In contrast, the opposite is true for Pol ε, which has an invariant methionine at the same position (Met644 in yeast). When Met644 is changed to leucine, M644L Pol ε becomes more like Pol δ, in that it incorporates fewer ribonucleotides (Nick McElhinny et al., 2010b). In other words, wild type Pol ε is only one amino acid away from being able to more effectively exclude ribonucleotides from DNA, yet Met644 is strictly conserved in Pol ε from many organisms (Figure 3). This suggests that there may be positive selective advantages to Pol ε incorporation of ribonucleotides into the nascent leading strand. Among several possibilities we discussed previously (Nick McElhinny et al., 2010c), this study provides evidence for one advantage, i.e., using the transient presence of a ribonucleotide to stabilize the genome by signaling for MMR, followed by ribonucleotide removal (Nick McElhinny et al., 2010b; Sparks et al., 2012) to prevent short deletions via a post-replication pathway initiated by endonucleolytic cleavage by topoisomerase 1 (Kim et al., 2011).

EXPERIMENTAL PROCEDURES

Strains used in this study

All *Saccharomyces cerevisiae* strains used in this study may be found in Table S5, along with associated references.

Stable rNMP incorporation *in vitro* measurements

Assays were performed as in (Nick McElhinny et al., 2010a). The average percentages of alkali-sensitive product for each indicated DNA polymerase was calculated using data from two experiments (error bars indicate the range). Data for four-subunit wild-type and M644G Pol ε are from (Nick McElhinny et al., 2010b; Williams et al., 2012). Wild-type and L612M Pol δ were purified as described (Burgers and Gerik, 1998).

Probing for ribonucleotides in yeast genomic DNA *in vivo*

Genomic DNA was isolated from asynchronously growing strains in the exponential phase of growth using the Epicentre Yeast DNA purification kit. Five μg of DNA were subjected to alkaline-lysis by treatment with 0.3 M KOH for 2 hours at 55 °C. Alkaline-agarose electrophoresis was performed as described (Nick McElhinny et al., 2010b) and the DNA was transferred to a charged nylon membrane by capillary action and subjected to Southern analysis. Probing was performed using single-strand radiolabeled probes that anneal to either the nascent leading or nascent lagging strand of the *URA3* reporter gene inserted in orientation 1 (OR1) at the *AGP1* locus on chromosome III.

Quantitative analysis of strand-specific alkaline-hydrolysis fragmentation patterns

Fluorescence intensity was quantified for each alkali gel lane (Figure 1C) in 0.1 mm increments in order to create a curve – $I(d_i)$ – of intensity versus migration distance (examples in Figure S1A–B). DNA ladders were used to build a standard curve for each gel. The migration distance of each standard, d, was related to the standard size, s (in base pairs), by the relation:

$$d = ae^{-b}. \quad \text{Equation 1.}$$

This function was fit to each standard curve via least squares regression. Each point, i, in $I(d_i)$ was transformed via the following function:

$$s_i = 1\left(\mathrm{n}\frac{a}{d_i}\right)/b. \quad \text{Equation 2.}$$

This resulted in curves – $I(s_i)$ – of intensity versus hydrolysis fragment size (examples in Figure S1C–D). Due to the logarithmic transformation, the width of bins represented by each point differ by up to 100-fold. This effect is corrected by first finding the bin width, w, for each point via

$$w_i = (s_{i-1} - s_i)/2 - (s_i - s_{i+1})/2 = (s_{i-1} + s_{i+1} - 2s_i)/2, \quad \text{Equation 3.}$$

and then converting to the average intensity per minimum bin width, $\bar{I}(s_i)$, for each point via

$$\bar{I}(s_i) = I(s_i)\frac{w_{\min}}{w_i}. \quad \text{Equation 4.}$$

$\bar{I}(s_i)$ is then converted to the fraction of fragments of a given size, $f(s_i)$ (examples in Figure S1E–F and I–J), by normalizing versus total lane intensity, I_T.

$$I_T = \sum_{i=1}^{n} I(s_i) \quad \text{Equation 5.}$$

$$f(s_i) = \bar{I}(s_i)/I_T \quad \text{Equation 6.}$$

In many cases observed in this study, $f(s_i)$ is clearly bimodal. Monte Carlo simulations of *Saccharomyces cerevisiae* chromosome 3 fragmentation were performed, assuming probe location at the *AGP1* locus, 1.5 kbp from *ARS306* (Figure 1B; Supplemental Methods: Alkaline hydrolysis). The simulated $f(s_i)$ curves each fit to a Weibull distribution, $W_i(s)$:

$$W_i(s) = A_i\frac{\alpha_i}{\beta_i}e^{-\left(\frac{s}{\beta_i}\right)^{\alpha_i}}\left(\frac{s}{\beta_i}\right)^{\alpha_i-1}. \quad \text{Equation 7.}$$

The bimodal observed $f(s_i)$ curves each fit to a sum of two Weibull distributions (examples in Figure S1G–H), representing a high-mobility population (*H*; small fragments) and a low-mobility population (*L*; large fragments). The high-mobility fraction, f_H, may be calculated from the scaling parameters, A_H and A_L via:

$$f_H = \frac{A_H}{A_H + A_L}. \quad \text{Equation 8.}$$

High-mobility fractions are shown in Figure 1E.

Forward mutation assays

Mutation rates for each strain were estimated from *URA3* mutation frequencies that were collected as in (Nick McElhinny et al., 2008; Pursell et al., 2007).

URA3 mutation spectra

URA3 mutation spectra were collected as per (Nick McElhinny et al., 2008; Pursell et al., 2007).

Mutation rates and correction factor calculations

Mutation rates and mismatch repair correction factors for specific mutation types (i.e. transitions and indels) mutation were calculated for each spectrum *URA3* as per (Lujan et al., 2012).

Statistical analysis of mismatch repair efficiencies

In order to show differences in mismatch repair between RNH201 and rnh201Δ strains, p-values for comparison of correction factors were assigned (Figure 2). These were estimated as the proportion of at least 1000 Monte Carlo simulated data sets (both fluctuation and

spectral results) that resulted in correction factors exceeding the relevant comparators. For purposes of Monte Carlo simulations, forward mutation rates were assumed to follow log-normal distributions and mutation spectrum counts to follow binomial distributions, as per (Lujan et al., 2012).

Supplementary Material

Refer to Web version on PubMed Central for supplementary material.

Acknowledgments

We thank Jeffrey Stumpf and Kin Chan for helpful comments on the manuscript. We acknowledge the Molecular Genetics Core Facility at the National Institute of Environmental Health Sciences for sequence analysis of 5-FOA-resistant mutants. This work was supported by Project Z01 ES065070 to T.A.K. from the Division of Intramural Research of the National Institutes of Health (NIH), National Institute of Environmental Health Sciences (NIEHS).

References

Bubeck D, Reijns MA, Graham SC, Astell KR, Jones EY, Jackson AP. PCNA directs type 2 RNase H activity on DNA replication and repair substrates. Nucleic Acids Res. 2011; 39:3652–3666. [PubMed: 21245041]

Burgers PM. Polymerase dynamics at the eukaryotic DNA replication fork. The Journal of biological chemistry. 2009; 284:4041–4045. [PubMed: 18835809]

Burgers PM, Gerik KJ. Structure and processivity of two forms of Saccharomyces cerevisiae DNA polymerase delta. J Biol Chem. 1998; 273:19756–19762. [PubMed: 9677406]

Cho JE, Kim N, Li YC, Jinks-Robertson S. Two distinct mechanisms of Topoisomerase 1-dependent mutagenesis in yeast. DNA repair.

Chon H, Vassilev A, DePamphilis ML, Zhao Y, Zhang J, Burgers PM, Crouch RJ, Cerritelli SM. Contributions of the two accessory subunits, RNASEH2B and RNASEH2C, to the activity and properties of the human RNase H2 complex. Nucleic Acids Res. 2009; 37:96–110. [PubMed: 19015152]

Clark AB, Lujan SA, Kissling GE, Kunkel TA. Mismatch repair-independent tandem repeat sequence instability resulting from ribonucleotide incorporation by DNA polymerase epsilon. DNA Repair (Amst). 2011; 10:476–482. [PubMed: 21414850]

Eder PS, Walder JA. Ribonuclease H from K562 human erythroleukemia cells. Purification, characterization, and substrate specificity. J Biol Chem. 1991; 266:6472–6479. [PubMed: 1706718]

Eder PS, Walder RY, Walder JA. Substrate specificity of human RNase H1 and its role in excision repair of ribose residues misincorporated in DNA. Biochimie. 1993; 75:123–126. [PubMed: 8389211]

Fang WH, Modrich P. Human strand-specific mismatch repair occurs by a bidirectional mechanism similar to that of the bacterial reaction. J Biol Chem. 1993; 268:11838–11844. [PubMed: 8505312]

Holmes J Jr. Clark S, Modrich P. Strand-specific mismatch correction in nuclear extracts of human and Drosophila melanogaster cell lines. Proc Natl Acad Sci U S A. 1990; 87:5837–5841. [PubMed: 2116007]

Hombauer H, Campbell CS, Smith CE, Desai A, Kolodner RD. Visualization of eukaryotic DNA mismatch repair reveals distinct recognition and repair intermediates. Cell. 2011; 147:1040–1053. [PubMed: 22118461]

Iyer RR, Pluciennik A, Burdett V, Modrich PL. DNA mismatch repair: functions and mechanisms. Chem Rev. 2006; 106:302–323. [PubMed: 16464007]

Kadyrov FA, Dzantiev L, Constantin N, Modrich P. Endonucleolytic function of MutLalpha in human mismatch repair. Cell. 2006; 126:297–308. [PubMed: 16873062]

Kadyrov FA, Genschel J, Fang Y, Penland E, Edelmann W, Modrich P. A possible mechanism for exonuclease 1-independent eukaryotic mismatch repair. Proc Natl Acad Sci U S A. 2009; 106:8495–8500. [PubMed: 19420220]

Kadyrov FA, Holmes SF, Arana ME, Lukianova OA, O'Donnell M, Kunkel TA, Modrich P. Saccharomyces cerevisiae MutLalpha is a mismatch repair endonuclease. J Biol Chem. 2007; 282:37181–37190. [PubMed: 17951253]

Kim N, Huang SN, Williams JS, Li YC, Clark AB, Cho JE, Kunkel TA, Pommier Y, Jinks-Robertson S. Mutagenic processing of ribonucleotides in DNA by yeast topoisomerase I. Science (New York, N.Y. 2011; 332:1561–1564.

Kleczkowska HE, Marra G, Lettieri T, Jiricny J. hMSH3 and hMSH6 interact with PCNA and colocalize with it to replication foci. Genes Dev. 2001; 15:724–736. [PubMed: 11274057]

Kunkel TA, Erie DA. DNA mismatch repair. Annu Rev Biochem. 2005; 74:681–710. [PubMed: 15952900]

Larrea AA, Lujan SA, Nick McElhinny SA, Mieczkowski PA, Resnick MA, Gordenin DA, Kunkel TA. Genome-wide model for the normal eukaryotic DNA replication fork. Proc Natl Acad Sci U S A. 2010; 107:17674–17679. [PubMed: 20876092]

Lujan SA, Williams JS, Pursell ZF, Abdulovic-Cui AA, Clark AB, Nick McElhinny SA, Kunkel TA. Mismatch repair balances leading and lagging strand DNA replication fidelity. PLoS Genet. 2012; 8:e1003016. [PubMed: 23071460]

Miyabe I, Kunkel TA, Carr AM. The major roles of DNA polymerases epsilon and delta at the eukaryotic replication fork are evolutionarily conserved. PLoS Genet. 2011; 7:e1002407. [PubMed: 22144917]

Modrich P, Lahue R. Mismatch repair in replication fidelity, genetic recombination, and cancer biology. Annu Rev Biochem. 1996; 65:101–133. [PubMed: 8811176]

Nick McElhinny SA, Gordenin DA, Stith CM, Burgers PM, Kunkel TA. Division of labor at the eukaryotic replication fork. Mol Cell. 2008; 30:137–144. [PubMed: 18439893]

Nick McElhinny SA, Kissling GE, Kunkel TA. Differential correction of lagging-strand replication errors made by DNA polymerases {alpha} and {delta}. Proc Natl Acad Sci U S A. 2010a; 107:21070–21075. [PubMed: 21041657]

Nick McElhinny SA, Kumar D, Clark AB, Watt DL, Watts BE, Lundstrom EB, Johansson E, Chabes A, Kunkel TA. Genome instability due to ribonucleotide incorporation into DNA. Nat Chem Biol. 2010b; 6:774–781. [PubMed: 20729855]

Nick McElhinny SA, Stith CM, Burgers PM, Kunkel TA. Inefficient proofreading and biased error rates during inaccurate DNA synthesis by a mutant derivative of Saccharomyces cerevisiae DNA polymerase delta. J Biol Chem. 2007; 282:2324–2332. [PubMed: 17121822]

Nick McElhinny SA, Watts B, Kumar D, Watt DL, Lundström E-B, Burgers PMJ, Johansson E, Chabes A, Kunkel TA. Abundant ribonucleotide incorporation into DNA by yeast replicative polymerases. Proc Natl Acad Sci U S A. 2010c; 107:4949–4954. [PubMed: 20194773]

Pavlov YI, Mian IM, Kunkel TA. Evidence for preferential mismatch repair of lagging strand DNA replication errors in yeast. Curr Biol. 2003; 13:744–748. [PubMed: 12725731]

Pavlov YI, Newlon CS, Kunkel TA. Yeast origins establish a strand bias for replicational mutagenesis. Mol Cell. 2002; 10:207–213. [PubMed: 12150920]

Pluciennik A, Dzantiev L, Iyer RR, Constantin N, Kadyrov FA, Modrich P. PCNA function in the activation and strand direction of MutLalpha endonuclease in mismatch repair. Proc Natl Acad Sci U S A. 2010; 107:16066–16071. [PubMed: 20713735]

Pursell ZF, Isoz I, Lundstrom EB, Johansson E, Kunkel TA. Yeast DNA polymerase epsilon participates in leading-strand DNA replication. Science (New York, N.Y. 2007; 317:127–130.

Rydberg B, Game J. Excision of misincorporated ribonucleotides in DNA by RNase H (type 2) and FEN-1 in cell-free extracts. Proc Natl Acad Sci U S A. 2002; 99:16654–16659. [PubMed: 12475934]

Smith DJ, Whitehouse I. Intrinsic coupling of lagging-strand synthesis to chromatin assembly. Nature. 2012; 483:434–438. [PubMed: 22419157]

Sparks JL, Chon H, Cerritelli SM, Kunkel TA, Johansson E, Crouch RJ, Burgers PM. RNase H2-Initiated Ribonucleotide Excision Repair. Mol Cell. 2012; 47:980–986. [PubMed: 22864116]

Thomas DC, Roberts JD, Kunkel TA. Heteroduplex repair in extracts of human HeLa cells. J Biol Chem. 1991; 266:3744–3751. [PubMed: 1995629]

Tran HT, Gordenin DA, Resnick MA. The 3'-->5' exonucleases of DNA polymerases delta and epsilon and the 5'-->3' exonuclease Exo1 have major roles in postreplication mutation avoidance in Saccharomyces cerevisiae. Mol Cell Biol. 1999; 19:2000–2007. [PubMed: 10022887]

Umar A, Buermeyer AB, Simon JA, Thomas DC, Clark AB, Liskay RM, Kunkel TA. Requirement for PCNA in DNA mismatch repair at a step preceding DNA resynthesis. Cell. 1996; 87:65–73. [PubMed: 8858149]

Williams JS, Clausen AR, Nick McElhinny SA, Watts BE, Johansson E, Kunkel TA. Proofreading of ribonucleotides inserted into DNA by yeast DNA polymerase epsilon. DNA Repair (Amst). 2012; 11:649–656. [PubMed: 22682724]

Highlights

- Deletion of *RNH201* causes a decrease in mismatch repair efficiency.
- This effect is specific to errors made on the nascent leading strand.

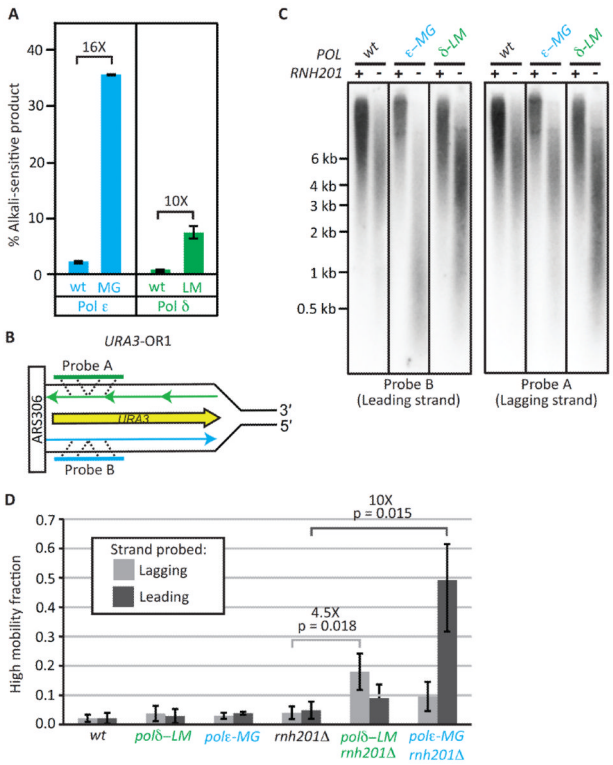

Figure 1. Ribonucleotide incorporation by Pols ε and δ

(A) Stable incorporation of ribonucleotides into DNA was measured *in vitro* as described (Nick McElhinny et al., 2010c). The average percentages of alkali-sensitive product for two experiments ± the range are displayed. (**B**) The orientation of the *URA3* reporter with respect to coding sequence is shown. The nascent leading strand synthesized by Pol ε is in blue and the nascent lagging strand synthesized by Pol δ is in green. (**C**) Strand-specific probing for alkali-sensitive sites in genomic DNA. DNA was subjected to alkaline hydrolysis, alkaline-agarose electrophoresis and analysis by Southern blotting using radiolabeled probes specific for nascent leading (Probe B) or nascent lagging (Probe A) strand DNA. DNA marker sizes are indicated on the left. Higher mobility (smaller) fragments reveal the presence of unrepaired ribonucleotides due to lack of RNase H2 activity. (**D**) Fraction of hydrolysis fragments present in the high mobility peak (see Figure S1 and Experimental Procedures). Error bars represent 95% C.I.

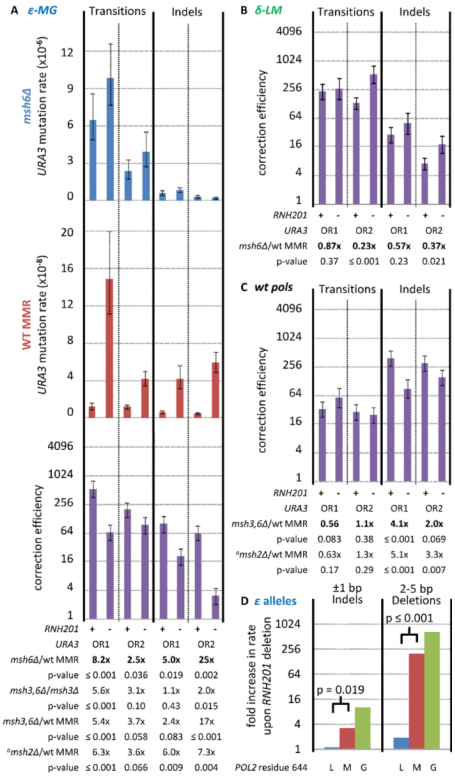

Figure 2. The effect of *RNH201* deletion on mutation rates and correction factors

Error bars represent 95% C.I. (**A**) *URA3* mutation rates are shown for *pol2-M644G* strains with *MSH6* deleted (*msh6*Δ; blue bars) or wild type mismatch repair (WT MMR; red bars). Correction factors (correction efficiency; purple bars), are ratios of mutation rates (*msh6*Δ : *MSH6*). Rates and correction factors are shown for transitions (left) and indels (right). RNase H2 status (*RNH201* = "+"; *rnh201*Δ = "−") and *URA3* orientation are indicated below the charts. Ratios of correction factors (*RNH201* : *rnh201*Δ) and the corresponding p-values (indicating confidence that correction factors differ) are shown at bottom, beginning with ratios derived from correction factors shown ("*msh6*Δ/wt MMR"; Table 1) and continuing for strains with different MMR deficiencies (see Tables S1–S2). [a]No measurements were made in an *msh2*Δ *rnh201*Δ strain (see Table S2). (**B**) As per the bottom of panel A, but for the *pol3-L612M* mutator background (δ-*LM*; see Table S3). (**C**) As per panel B, but for the wild type polymerase background (*wt pols*; see Table S4). (**D**) Fold increases in single-base indel and 2–5 bp tandem repeat deletion rates - due to *RNH201* deletion - are shown for three Pol ε variants: M644L Pol ε (blue bars; see Table S7), wild type Pol ε (red bars), and M644G Pol ε (green bars).

Clade					Polymerase ε		Polymerase δ	
Eukarya	Unikonta	Opisthokonta	Fungi	Ascomycota	SMYPNIM	188	SLYPSI(I,M)	182
				Basidomycota	AMYPNIM	28	SLYPSIM	23
				other	AMYPNII	2	SLYPSIM	2
			Microsporidia		AMYPNII	[a]4	SLYPSI(I,M)	5
			Metazoa		AMYPNII	165	SLYPSI(I,M)	[b]149
			other		AMYPNII	10	SLYPSIM	4
		Amoebozoa			AMYPNII	12	SLYPSIM	6
	Bikonta	Archaeplastida			AMYPNII	44	SLYPSIM	32
		other			AMYPNII	46	SLYPSI(I,M)	41

Figure 3. Conservation in the polymerase active site of Pols ε and δ

Organisms are grouped by clade with organism counts to the right of each sequence. [a]Putative Polymerase ε from *Nosema ceranae* [SLYTDII]. [b]Polymerases δ from *Trichoplax ahaerens* [SLYP(TII,SII,SIM,SVM)] and *Loxodonta africana* [SMYPSIV].

Mol Cell. Author manuscript; available in PMC 2014 May 09.

Table 1

pol2-M644G mutation rates in two *URA3* orientations ± *MSH6* and/or *RNH201*.

***pol2-M644G msh6Δ*/wt MMR**			**mutation rate(×10^{-7})**	**95% confidence**	**5-FOA^{R} mutants**	**no *URA3* change**	***URA3* mutations**	**Transitions**		**Frameshifts**	
								#	**rate**	**#**	**rate**
***URA3* orientation 1**	***RNH201***	wt MMR	1.7	(1.3–2.3)	342	105	237	24	0.12	12	0.060
		msh6Δ	110	(82–150)	219	26	205	130	65	12	6.0
		correction factors							**550×**		**100×**
	***rnh201* Δ**	wt MMR	7.6	(4.3–10)	128	4	125	25	1.5	7	0.42
		msh6Δ	170	(130–220)	141	10	133	82	99	7	8.4
		correction factors							**67×**		**20×**
	***RNH201/rnh201Δ* correction factor ratios**								**8.2**		**5.0**
	p-values								≤ 0.001		0.019
***URA3* orientation 2**	***RNH201***	wt MMR	0.83	(0.71–0.96)	246	123	124	36	0.12	14	0.047
		msh6Δ	54	(40–75)	181	38	149	79	24	10	3.0
		correction factors							**190×**		**63×**
	***rnh201* Δ**	wt MMR	14	(9.8–20)	138	0	138	5	0.51	7	0.71
		msh6Δ	81	(57–110)	134	20	126	65	39	3	1.8
		correction factors							**77×**		**2.6×**
	RNH201/rnh201Δ correction factor ratios								**2.5**		**25**
	p-values								0.036		0.002

For comparison, all rates are listed by strain in Table S6. All rates are multiplied by 10^{7}. Correction factors are compared in Figure 2A, listed as "*msh6*Δ/wt MMR". Strain origins and related references may be found in Table S5. Among the mutants with no sequence change in the *URA3* open reading frame, some may have arisen due to sequence changes in the *URA3* promoter or in another gene that affects resistance to 5-FOA. Because these mutants contribute to the overall mutation rate, they are included in the calculation of rates for individual mutation classes.